Experimental investigation of microstructural changes in soils eroded by suffusion using X-ray tomography

Cong Doan Nguyen, Nadia Benahmed, Edward Andò, Luc Sibille, Pierre Philippe

Experimental investigation of micro-structural changes of soils eroded by suffusion using x-ray tomography

Cong Doan Nguyen[a], Nadia Benahmed[a1], Edward Andò[b], Luc Sibille[b], Pierre Philippe[a]

[a]*IRSTEA, Research Unit RECOVER, 3275 route de Cézanne CS 40061, 13182 Aix-en-Provence Cedex 5, France*

[b]*University Grenoble Alpes, CNRS, Grenoble INP, 3SR, F-38000 Grenoble, France*

Abstract

Internal erosion is a complex phenomenon which represents one of the main risks to the safety of earthen hydraulic structures such as embankment dams, dikes or levees. Its occurrence may cause instability and failure of these structures with consequences that can be dramatic. The specific mode of erosion by suffusion is the one characterized by seepage flow induced erosion and the subsequent migration of the finest soil particles through the surrounding soil matrix mostly constituted of large grains. Such a phenomenon can lead to a modification of the initial microstructure and, hence, to a change in the physical, hydraulic and mechanical properties of the soil.

A direct comparison of the mechanical behaviour of soil before and after erosion is often used to investigate the impact of internal erosion on soil strength (shear strength at peak and critical state) using triaxial tests. However, the obtained results are somehow contradictory, as for instance in Chang's study [1], where it is concluded that the drained strength of eroded soil decreases compared to non-eroded soil while both Xiao and Shwiyhat [2] and Ke and Takahashi [3] have come to the opposite conclusion. A plausible explanation of these contradictions might be attributed to the rather heterogeneous nature of the suffusion process and to the way the coarse and fine grains are rearranged afterwards leading to a heterogeneous soil structure, a point that, for now, is not taken into account, nor even mentioned, in the existing analyses.

In the present study, x-ray computed tomography (x-ray CT) is used to follow the microstructure evolution of a granular soil during a suffusion test, and therefore, to capture the induced micro-structural changes. The images obtained from x-ray CT reveal indeed that fine particles erosion is obviously not homogeneous, highlighting the existence of preferential flow paths that lead to a heterogeneous sample in terms of fine particles, void ratio and inter-granular void ratio distribution.

Keywords: internal erosion; suffusion; microstructure; heterogeneity; x-ray computed tomography.

[1] *nadia.benahmed@irstea.fr; +33(0)4 42 66 99 04*

1 Introduction

Internal erosion of soil induced by seepage flow is considered as the main cause of degradation and failure of earthen structures (dikes, earth dams, etc.). It is assumed that four types of erosional processes can be encountered during the internal erosion of water-retaining structures or their foundations: suffusion, backward erosion, contact erosion and concentrated leak erosion [4, 5]. They are all related to intense seepage flow within the earthen structure. In the case of suffusion that is in the scope of the present study, the smallest soil particles are detached and transported by the interstitial water flow through the surrounding soil matrix, mostly constituted of large grains. The strength of the seepage flow and the nature of the materials jointly determine the vulnerability against suffusion within a given embankment dam or dike section. Worrying vulnerability is observed under the following conditions: first, high enough seepage forces are needed, providing sufficient energy and momentum to detach particles from the soil structure; second, the eroded particles should have the possibility to be substantially transported within the porous material by the water flow, which requires the detached particles sizes to be mostly smaller than the ones of the constrictions between the coarser particles of the soil's skeleton. Soils vulnerable to suffusion are denominated as "internally unstable" [6-8].

The internal erosion potential of different soils has been investigated experimentally by a number of researchers. The related results give an indication about the vulnerability of soils with respect to suffusion in terms of empirical rules that can be prescribed by the particles size distribution curve [6, 9, 12], the constrictions size distribution [13-15], the particle shape [16], the effective stress [17, 18], and the hydraulic gradient [19].

The direct observation of suffusion phenomenon is the loss of fine particles and the settlement during the suffusion test. These changes generally lead to an increase in the porosity and possibly a decrease in sample volume of the soil sample [1, 2, 20]. Besides, the coarse grains may rearrange, possibly under fluid flow stresses, but above all, due to the progressive disappearance of the stabilizing presence of fine particles. The initial soil fabric may thus be changed during suffusion process with a possible impact on the subsequent mechanical behavior.

Changes in the mechanical response of a soil before and after erosion are often used to investigate and quantify the effect of internal erosion on soil strength (shear strength at peak/critical state) using triaxial tests. Chang and Zhang [1] first found that the drained soil strength decreases after the erosion, whereas Xiao and Shwiyhat [2] and later Ke and Takahashi [3] showed that the undrained peak deviator stress of eroded soil is larger than the soil without erosion. As pointed out, the results from these previous experimental investigations on the mechanical consequences of internal erosion are somewhat contradictory. The potential reasons for this might be related to the rather heterogeneous nature of the suffusion process and to the change in soil fabric resulting from selective suffusion [21]. However, the suffusion test results in literature give only a macroscopic point of view and fail to quantify the suffusion phenomenon at the scale of the soil's induced heterogeneities. Yet suffusion is precisely expected to initiate at some specific locations where preferential flows occur and then to progress over a certain area within the soil sample as illustrated in **Fig. 1** regarding a typical experiment of the present study to be detailed

hereafter. The same kind of transverse heterogeneities (i.e. perpendicularly to the main fluid flow direction) induced by suffusion was also observed by Sail et al. [22], Luo et al. [23], and Israr et al. [24]. In addition, longitudinal heterogeneities (i.e. in the direction of the flow) within a soil specimen subject to a suffusion test under constant flow rate are strongly suspected from measurements of the overall hydraulic gradient along the specimen. Rather sharp increases or decreases of the global hydraulic gradient versus time are often observed and were attributed to clogging and subsequent wash-out of fine particle in some area of the sample, which thus appear as heterogeneities in the direction of flow [3, 23]. Thus, particle scale analyses of eroded soil are necessary to reveal the microstructural change induced by suffusion and further relate it to the soil's mechanical behavior. However, few experimental investigations into the suffusion process at this local scale have been reported in the literature [25, 26] and this is the main motivation of the present study.

In this paper, microscopic observations of a soil sample during a suffusion test are investigated by using x-ray tomography with the aim of better understanding the suffusion consequences. The methodology for in-operando x-ray tomography during a suffusion test is firstly presented in Section 2. Next the image processing techniques used to extract micro-scale measurements from the 3D reconstituted images is detailed in Section 3. Then, the evolution of these micro-scale measurements during the suffusion development are interpreted in Section 4 in terms of void ratio, inter-granular void ratio, fines content, and deformation fields. Finally, Section 5 summarizes the main outcomes of this study.

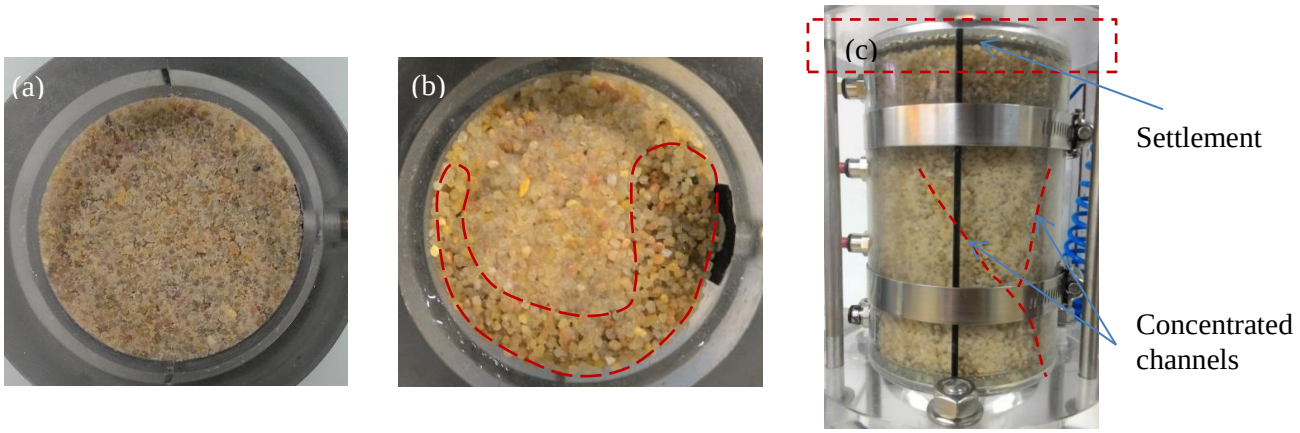

Fig. 1 Photography of suffusion process; (a): initial state; (b): high erosion zone (dash line); (c): concentrated channels of fines migration.

2 Microscopic investigation of suffusion development

2.1 Tested materials

In this study, a gap-graded soil is created by using a mixture of two different types of Hostun sand, namely HN 1/2.5 and HN34, which are granular siliceous materials with an angular to sub-angular grain shape. The HN 1/2.5 is the coarse fraction grains while the HN34 sand is considered as the erodible fine particles. These fine particles were used in a proportion of 25 % in mass or, equivalently, 25% in solid volume to form the mixture, named FC25.

It is worth noting that suffusion usually occurs in gap-graded granular soils due to their deficiency at certain grain sizes [19]. The potential of suffusion is controlled by the geometric properties of the soil's composition following the methods proposed by Kézdi [9], Kenney and Lau [6, 10] and Burenkova [11], among others. According to these criteria regarding suffusion occurrence, the reconstituted soil is indeed potentially unstable and vulnerable to internal erosion under seepage flow. The properties of these two sands are shown in Table 1 while **Fig. 3** provides their grain size distributions together with the one of the mixture.

Table 1 Sand particles size distribution parameters.

Properties	HN 34	HN 1/2.5	FC25
Specific gravity, ρ_s	2.65	2.65	2.65
Minimum particle size D_0 (mm)	0.1	0.63	0.1
Maximum particle size D_{100} (mm)	0.5	2.5	2.5
Median particle size, D_{50} (mm)	0.21	1.7	1.6
D'_{15}/d'_{85}	-	-	5
$(H/F)_{min}$	-	-	0.12
$h' = D_{90}/D_{60}$	-	-	1.24
$h'' = D_{90}/D_{15}$	-	-	9.13

D_X: denotes the maximum size of the smallest X% of the soils; D'_{15}: the maximum size of the smallest 15% of the coarse fraction (HN 1/2.5); d'_{85}: the maximum size of the smallest 85% of the fines fraction (HN34); $(H/F)_{min}$: F is the weight fraction of the soil finer than size *d* and H is the weight fraction of the soil in the size ranging from *d* to *4d*; $h' = D_{90}/D_{60}$ and $d'' = D_{90}/D_{15}$: conditional factor of uniformity.

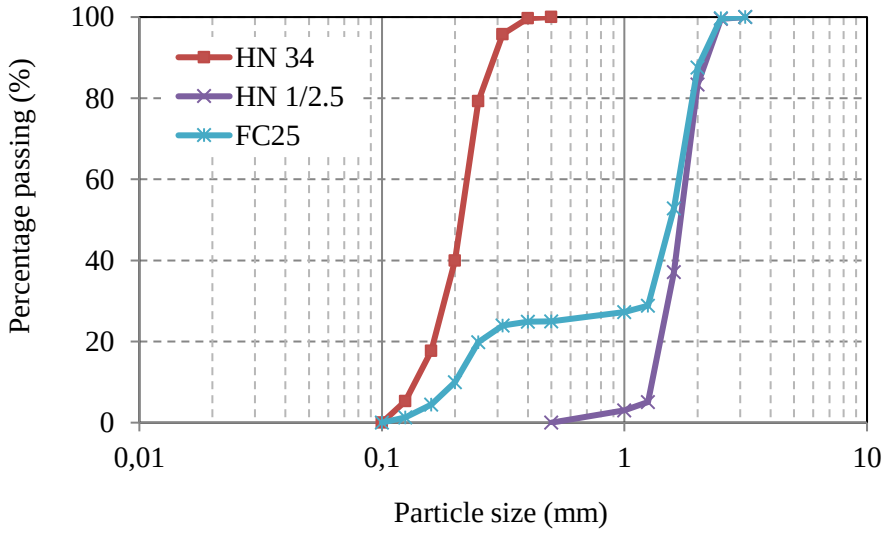

Fig. 2 Particle size distribution curves of the coarse sand (HN 1/2.5), the fine particles (HN34), and the mixture (FC25).

2.2 Suffusion permeameter and specimen preparation

To perform suffusion tests, for understanding the mechanism of this process during which the soil specimen will experience seepage-induced erosion and migration of fine particles, an apparatus called suffusion permeameter was developed and used in this study. The general layout of the apparatus is shown in **Fig. 3**. It consists of a cylindrical plexiglass cell allowing external visualization of the specimen, fitted with 4 slots longitudinally for pressure measurements. The inlet of the cell is connected to a Peristaltic Metering pump

(FLOWROW N375) which controls the water flow rate through the specimen from a water tank, while the outlet is connected to a soil particle collecting system placed inside the water tank.

The soil specimen is prepared inside the cell by the moist tamping method to prevent soil segregation [27, 28]. Briefly, the soil is compacted in seven successive layers of identical fixed height to reach the target dry density. Each layer represents a seventh of the total soil mass uniformly moistened by a few amount of water (5% in mass), and then compacted manually to the desired height using a graduated tamper. The final dimensions of the specimen are 70 mm in diameter and 140 mm in height. It is placed between 2 horizontal fixed layers of uniform glass beads (4 mm diameter) of about 12 mm height. These layers help break up the turbulent structures within the incoming flow to ensure an almost uniform and laminar flow through the specimen. Hence, the upper layer does not apply any stress on the sample. To reduce preferential flows between the inner wall and the soil, a rough transparent plastic sheet is beforehand inserted and set against the cell wall.

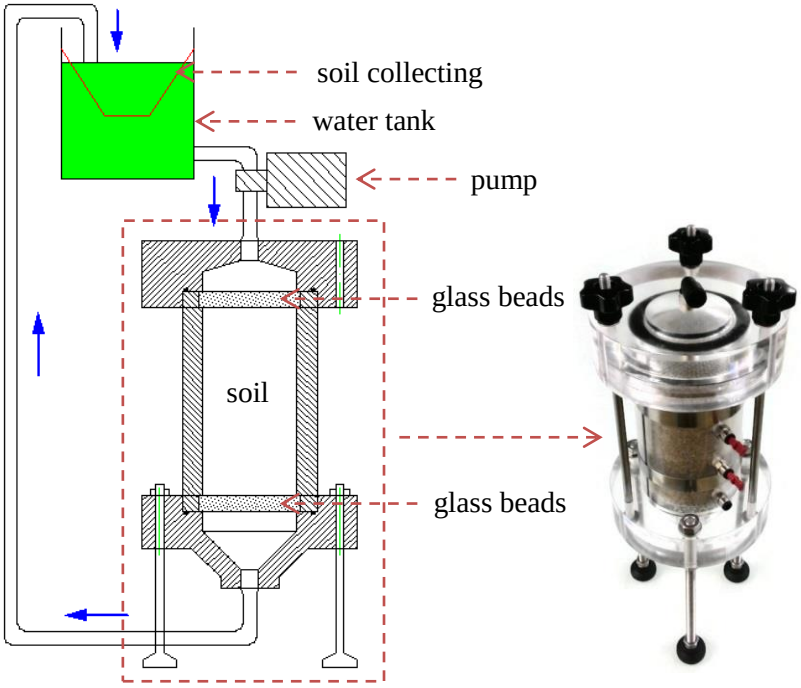

Fig. 3 Schematic diagram of the suffusion permeameter device.

2.3 Suffusion test with in-operando x-ray tomography

X-ray computed tomography (x-ray CT) aims to quantify a 3D field of x-ray attenuation (a material property linked to density). This is achieved by acquiring radiographic projections of the field under a large number of different angles, and reconstructing the 3D field using back projection. 3D field in reality is discretised into 3D volume elements (voxels, a voxel is 3D pixel). The x-ray scan system considered here is able to scan materials with resolutions ranging from a millimeter down to a few micrometers per pixel, depending on specimen size, detector resolution and rotation step size. The full-field measurement provided by x-rays is a revolutionary and increasingly used tool in experimental geomechanics. A spatial resolution greater than one millimeter was firstly used in the study of shear bands in granular soils by Desrues et al. [29]. Later, imaging at particle scale with a resolution of a few microns recently started to

be implemented in soil mechanics [30, 31]. Regarding more specifically internal erosion, x-ray CT was used for instance by Homberg et al. [32], Fonseca et al. [33], or more recently Dumberry at al. [34], Bianchi et al. [25] and Mehdizadeh et al. [26].

In the present study, the x-ray scanner in Laboratoire 3SR is used to investigate the consequences of suffusion within a granular sample subjected to an internal erosion test in the x-ray chamber (Fig. 4). The pixel size of the images is 90 µm/px. Compared to the size of the grains constituting the sample, quantified by the median particle sizes of fines d_{50} and of coarse grains D_{50}, the spatial resolution corresponds to $0.43d_{50}$ and $0.053D_{50}$, respectively, which is high enough to visualize individually the coarse grains but not the fine ones.

The study of suffusion using tomography being expensive and quite time consuming, the results presented in this paper concern an observation on a single experiment. Although only one sample was tested in the x-ray tomograph, the experiment carried out was repeated many times out of the tomograph with a good repeatability [35]. This suggests that the rather similar procedure adopted here in the tomography chamber is relevant and leads to the same type of microstructure evolution induced by suffusion.

The specimen preparation is presented in section 2.2. The suffusion test is conducted following a multi-step procedure and is divided into two main phases. The saturation phase consists of circulating Carbon dioxide CO_2 through the soil sample from bottom to top (upward direction) under a low pressure gradient, followed by distilled water at a very low flow rate. This step takes approximately 1 hour, which appears enough to ensure a good saturation quality since most of the interstitial air is first replaced by CO_2 that next dissolves completely in distilled water.

Afterwards, the erosion phase is launched and consists of applying a downward water flow at a constant flow rate that is progressively increased by steps as illustrated in **Fig. 5**. The value of flow rate is referred to as the Darcy velocity. The duration of each step is fixed to about 30 minutes. At the end of each step, an x-ray scan of the sample is performed while the eroded mass is collected and later weighted after drying. Note that the duration and the flow rate of each step were selected on the basis of a preliminary study where the critical flow rate for erosion onset has been identified: a flow rate of 0.15 cm/s was obtained for a similar sample, with same fine content and relative density. In the range of the flow rates investigated, the time for cessation of erosion was always less than 15 minutes and thus substantially smaller than the step duration. Four scans were performed in the present test, corresponding to 4 successive soil states during the step by step increasing flow rate procedure as depicted in **Fig. 5**: scan 01 is the scan after the saturation phase; scan 02 is the scan after applying a very low flow rate of 0.05 cm/s that is far below the critical flow rate; scan 03 and scan 04 are two scans obtained after the sample had been subjected to erosion with different eroding flow rate and duration. More precisely, scan 03 is performed after the sample was subjected to a flow rate of 0.25 cm/s for 30 minutes and scan 04 after an additional 30 minutes loading with a flow rate of 0.45 cm/s. The duration of each scan is approximately 30 minutes. The remaining masses of fines in the sample during these successive stages of the suffusion test are presented in Table 2. These masses are calculated from the eroded masses in the soil collecting system after drying and

weighting. These values will be useful later to assess the subsequent image processing detailed in the next following section.

3 Image processing

The reconstructed 16 bits images of the sample, for a given scan, is in the form of a 3D volume of 900×900×1700 voxels, corresponding to a physical volume of 81×81×153 mm. The visualized zone includes the entire soil sample. **Fig. 6** shows examples of the raw data in a median vertical section. The orientation of the plane is chosen so that it intercepts a most pronounced erosion zone as detailed later. Regarding the reference position of the sample in-between two scans, the meridian plane in Fig. 6 is orientated along the x-ray beam direction. Each voxel has a grey-level that represents the reconstructed x-ray attenuation at the corresponding point in the sample.

It is worth noting that the movement of fine particles may continue inside the sample after stopping the flow (i.e. during the scanning of the sample), however the quality of the obtained images, which are very clear, attests that this movement is insignificant (otherwise, the images must be blurry).

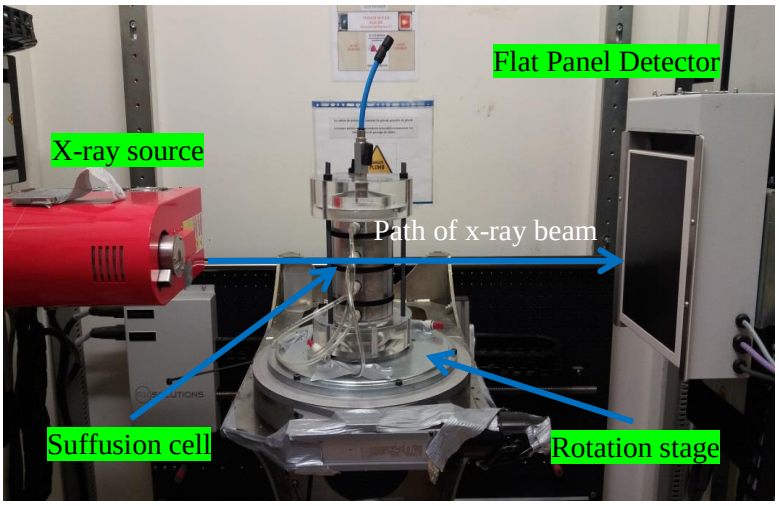

Fig. 4 Setup of the suffusion cell inside the x-ray chamber.

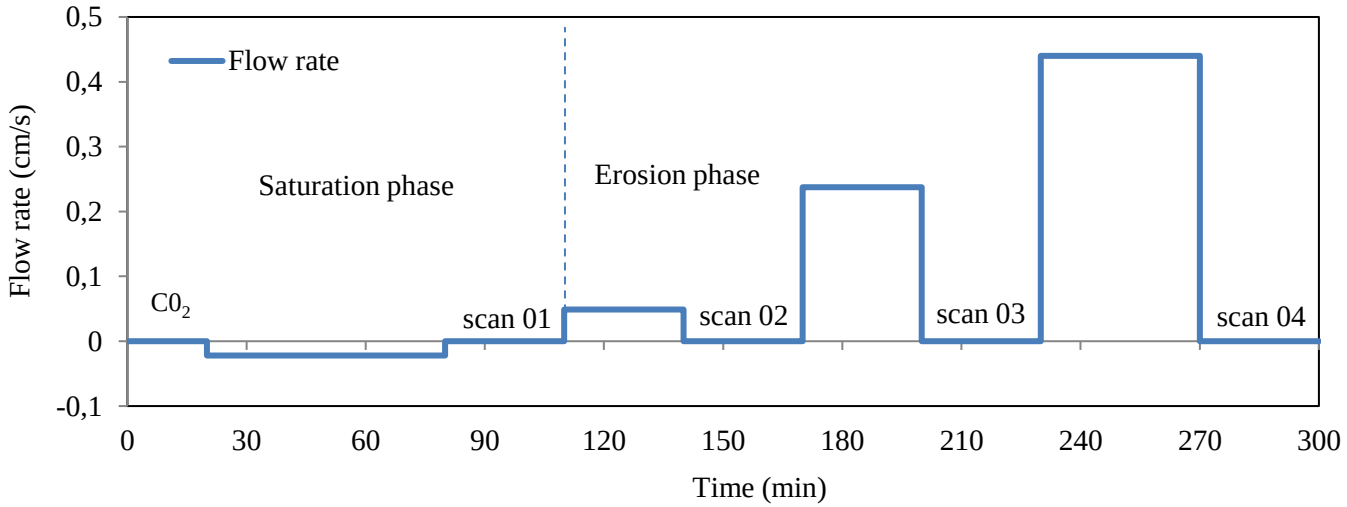

Fig. 5 Application of the flow rate by steps and location in time of the 4 successive scans.

Table 2 Volume of fine and coarse grains measured directly by weighting and estimated from image processing, by the end of each phase.

		scan 01	scan 02	scan 03	scan 04
Volume determined by weighing	Coarse grains (cm^3)	259.7	259.7	259.7	259.7
	Fines (cm^3)	85.7	85.7	65.1	39.0
	Coarse grains + fines (cm^3)	345.5	345.5	324.9	298.8
Volume determined by image processing	Coarse grains (cm^3)	259.8	259.7	259.6	259.8
	Fines (cm^3)	86.1	85.0	64.3	38.5
	Coarse grains + fines (cm^3)	345.9	344.8	323.9	298.4
	Sample volume (cm^3)	535.64	535.44	516.08	481.51
	Pore† (cm^3)	189.69	190.68	194.25	183.93
	(pore volume change, cm^3)	*(+0.0)*	*(+0.99)*	*(+4.75)*	*(-5.76)*

† The true pore volume (= sample volume – volume of fine particles – volume of coarse grains)

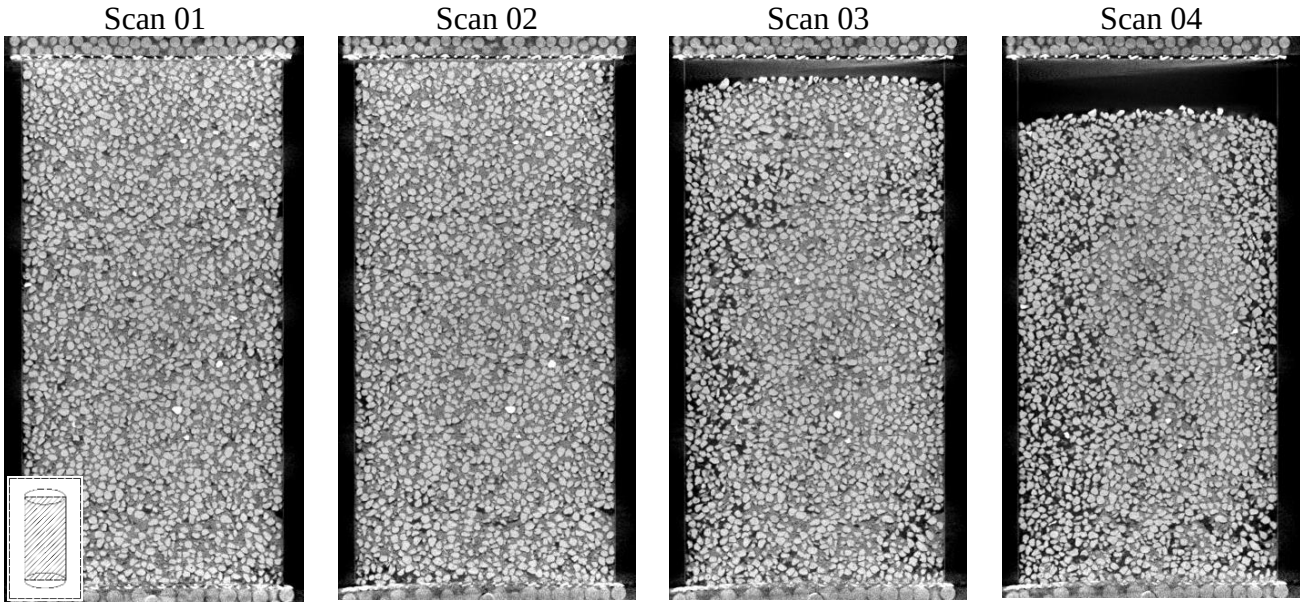

Fig. 6 Vertical sections of the 4 scans in the median plane of the sample.

In this study, Python programming language and open-source software ImageJ (specifically the Fiji distribution) have been used for image processing and forthcoming analysis. The following steps were successively implemented to post-process the raw 3D reconstructed images obtained from the 4 x-ray scans.

First, all the volume located outside of the soil sample is removed by imposing a zero greylevel. This cleaning is performed manually. From this step, the 3D reconstructed scan includes only coarse grains, fine particles and voids (pure water) inside the soil sample. Being made of the same material (silica sand), fine and coarse particles should be approximately represented by the same grey-level. However, as the size of a fine soil particle is small regarding the spatial resolution (d_{50} = 210 μm; voxel size = 0.43d_{50}), the grey-level of individual fine particles is difficult to measure accurately and only a mean grey-level of a mixture of fine particles and inter-fine water can be obtained. This results in an apparent grey-level lower than the one corresponding to a pure silica material (coarse grains). Consequently, the average grey-level value of

coarse grains and interstitial water remain almost unchanged in the whole sample and are rather easy to determine from a selection of voxels containing exclusively coarse grains or interstitial water, respectively. On the other hand, the grey-level of voxels including fine particles depends on the concentration of fine particles in each voxel volume, its value ranging from the mean grey-level of water to the mean grey-level of silica (coarse grains). The next steps consist in, first, identifying the coarse fraction from the sample and, second, correlating the grey-level in the inter-coarse granular space with the fine particles concentration.

By applying a given threshold on the grey-levels of the reconstructed image, one gets a binarised image composed of two phases: the inter-granular space and the coarse grains. The voxel volume being known, the total number of voxels included in the coarse granular phase gives a measurement of the volume of coarse grains in the sample. The threshold value is selected to match this coarse grain volume obtained from image processing with the one deduced from the mass of the coarse grains used to make the sample (see **Table 2**). An example of the resulting binarised images is shown in (Fig. 7b) where coarse grains are displayed in black.

In a second step, the grey-level of voxels included in the inter-granular space (identified in the previous step) is rescaled from 0, in order to be representative of the fine concentration is these voxels, according to the mean grey-level of pure water and pure silica (*i.e.*, grey-level of coarse grains). The rescaling is performed such that the grey-level of voxels including only pure water is now equal to 0 and the one of voxels filled with only silica is equal to 1. Then, the rescaled grey-level of any voxel including fines and water can be used to quantify the local content in fine particles, strictly comprised between 0 and 1, most values being lower than 0.7. The new images obtained this way are called calibrated images. Nevertheless, to clearly identify the coarse grains in the calibrated images, the masks of the coarse grains obtained from the binarised images are used by superimposition pixel by pixel on the calibrated images. Therefore, calibrated masked images are ultimately obtained where the grey-level of all coarse grains voxels is strictly equal to 1, while the grey-level of all other voxels varies from 0 (pure water) up to 1, according to the local concentration in fine particles. **Fig. 7**c shows an example of the filling rate of fines particles in the pores obtained in this way. Finally, the fine particles volume can be calculated by the following equation:

$$V_{FP} = \sum_{voxel \in inter-granular\ space} (V_{vox} \times I_{vox}^{c})$$

where V_{FP} is fine particles volume; V_{vox} is voxel size (90 µm); I_{vox}^{c} is concentration in fine particles of each voxel;

Qualitatively, **Fig. 8** shows the vertical section of each sample in the same median plane as the one presented in **Fig. 6**, using a color map for the degree of filling of fine particles in the inter-granular pores.

Quantitatively, **Table 2** shows the volumes of fine particles and coarse grains computed from the image processing which can be consistently compared to the values directly deduced by weighing. These results validate the ability of the proposed image processing to give local and quantitative information about the microstructure of the sample at the different stages of the suffusion process.

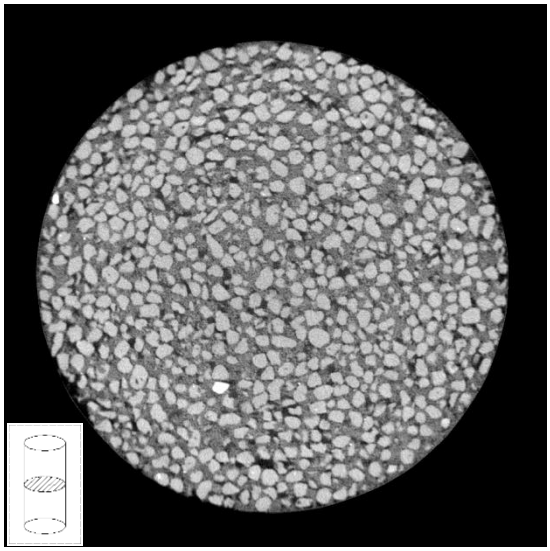

(a) Grey clean

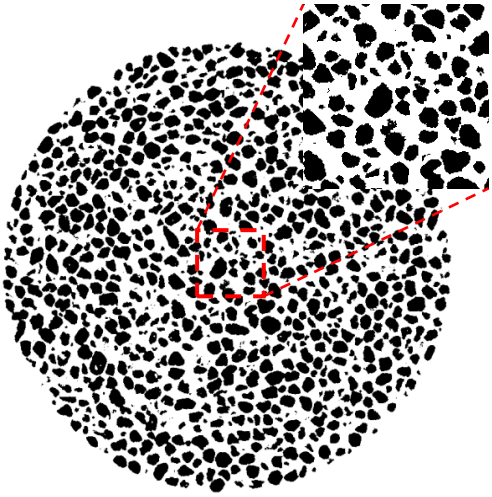

(b) binary and close labels to identify coarse grains

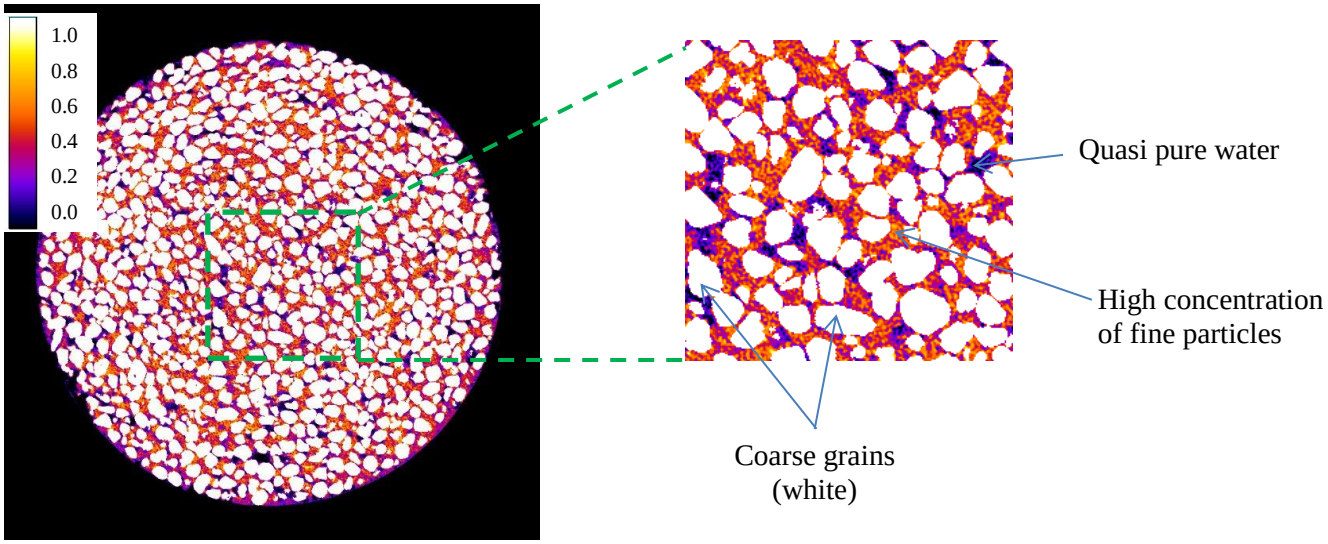

(c) filling rate of fine particles in the pores

Fig. 7 Successive steps for identification of the coarse granular phase and computation of the fine concentration.

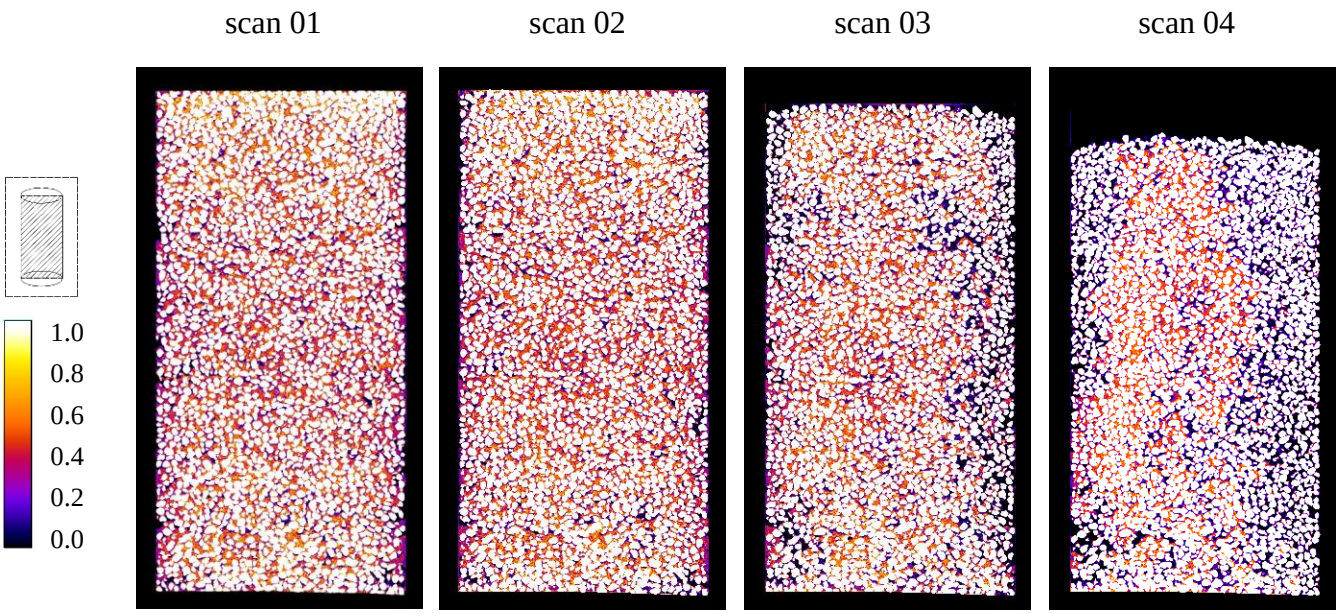

Fig. 8 Vertical sections in the median plane of the 4 scans after calibration of the fine solid concentration in the inter-granular space.

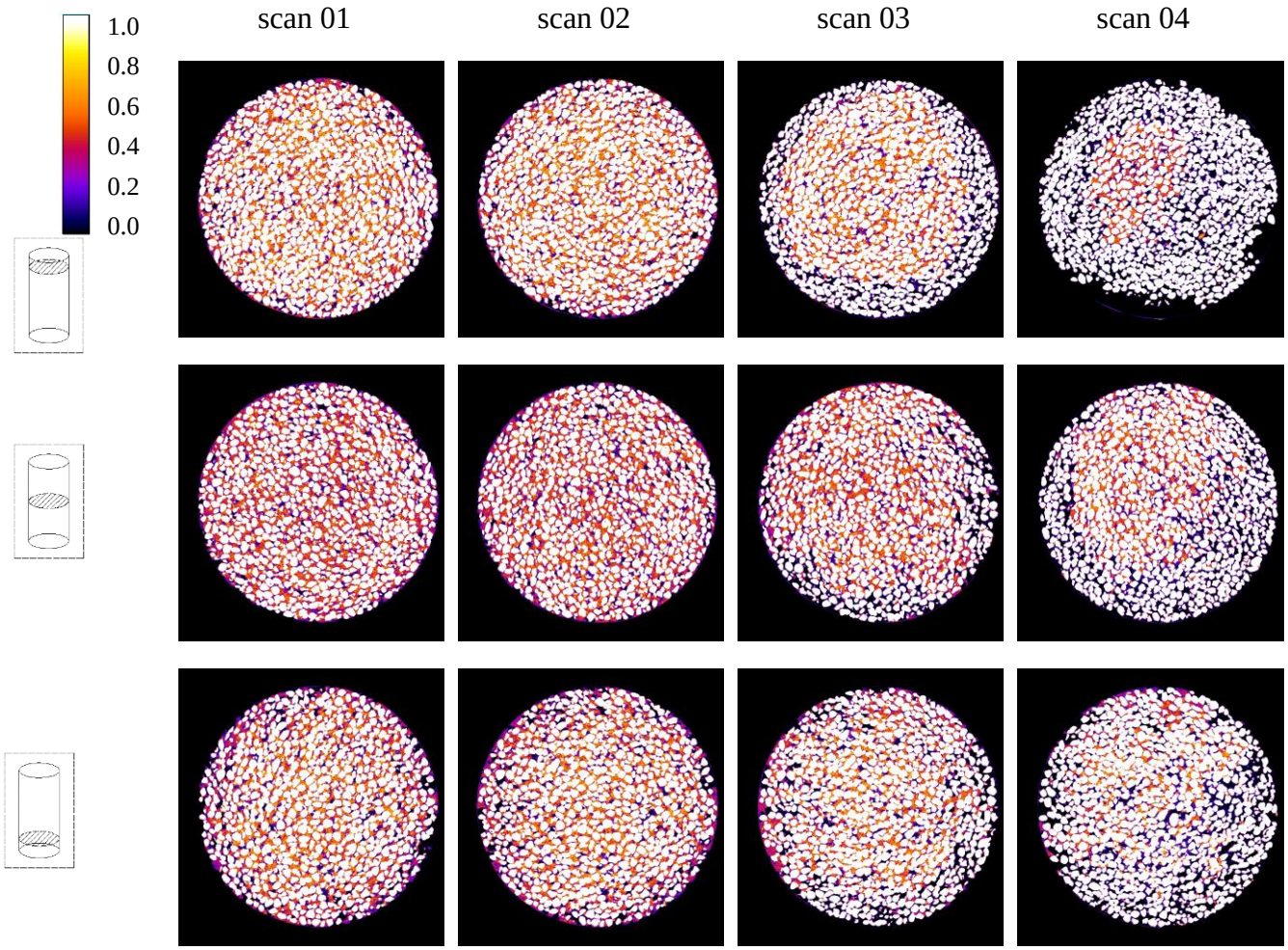

Fig. 9 Horizontal sections of the 4 scans at 3 different sample height positions after calibration of the fine solid concentration in the inter-granular space.

4 Description of suffusion development

From the vertical and horizontal sections (**Fig. 8** and **Fig. 9**), scan 01 and 02 show that fines loss is not distinguishable except at the bottom part of the sample where a slight change of fine particles concentration is observed. On the scan 03 and 04, the development of suffusion essentially takes place in a vertical channel, along the whole sample height, located at some positions around the lateral sample wall. This development starts around the sample periphery from the top and progress non uniformly to the bottom part. Such a development might be due to a stronger edge effect on the sample top layer directly in contact with the flow.

Subsequently, the preferential flows are formed in a rather random way, progressing longitudinally and horizontally as illustrated on the scan 3, by the erosion of fine particles which appears less concentrated on the perimeter of the horizontal section in the middle of the sample compared to that of the upper part. On the lower part, the preferential flows seem to converge, inducing a new depletion in fines concentration near the edge of the sample. This observation is more remarkable on the scan 04 when the erosion of fines becomes stronger.

One could notice the appearance of differential settlement induced by the erosion (under its own weight and the impact of downward flow) which is not symmetrical either on the axis or in the plane. This is consistent with the above observation related to the edge effect and the concentrated preferential paths close to the boundary.

5 Results and discussions

5.1 Global change of the sample physical state

The evolution of the state properties (density and fine content) of the sample during the suffusion test is firstly studied at the sample scale. From the results of the images processing detailed in the previous section, the following variables can be directly calculated: (*i*) the void ratio *e* that compares "void" volume (*i.e.* pure water) to solid volume; (*ii*) the inter-granular void ratio e_g that is similar to the void ratio except that fines are now considered as void; (*iii*) the fines content *f* that compares fine grains volume to total grains volume. These quantities, calculated for each scan for the whole sample, are presented in **Fig. 10**.

As expected, no visible global change is observed between scan 01 and scan 02 since no erosion in the sense of particles wash-out has occurred due to the very low flow rate. Then, from scan 02 to scan 04, as the flow rate is increased, the fine content globally decreases with the development of erosion which should lead to a more and more open microstructure. However, the settlement of the sample comes together with the erosion development. Such a settlement can be observed via the decreasing of the inter-granular void ratio corresponding to a compaction of the coarse granular skeleton. These two mechanisms are somehow in competition, with a slight predominance of the microstructure opening (due to fine departure) as the global void ratio is eventually slightly higher avec erosion than before (even if the coarse granular phase is itself denser).

By closely examining the change in real pore volume V_v, it can be stated whether erosion of fine particles (*i.e.*, increase of V_v) or granular skeleton settlement following the erosion process (i.e. decrease of V_v) is dominant. In that respect, **Table 2** shows that erosion is the main process modifying and loosening the

overall sample structure in scan 03. However, in this state, the pore volume is almost unchanged compared to the previous state implying that the increase of V_v by losing fine particles was almost equivalent to the decrease of V_v caused by granular skeleton settlement. In scan 04, even if in this case the erosion is greater than at the previous step, the sample is mainly affected by settlement and densification, resulting probably from an induced metastable skeleton structure. Nevertheless, the sample scale does not allow so far for more thorough analysis of erosion and subsequent settlement. An investigation at a more local scale is necessary as will be detailed in the next section.

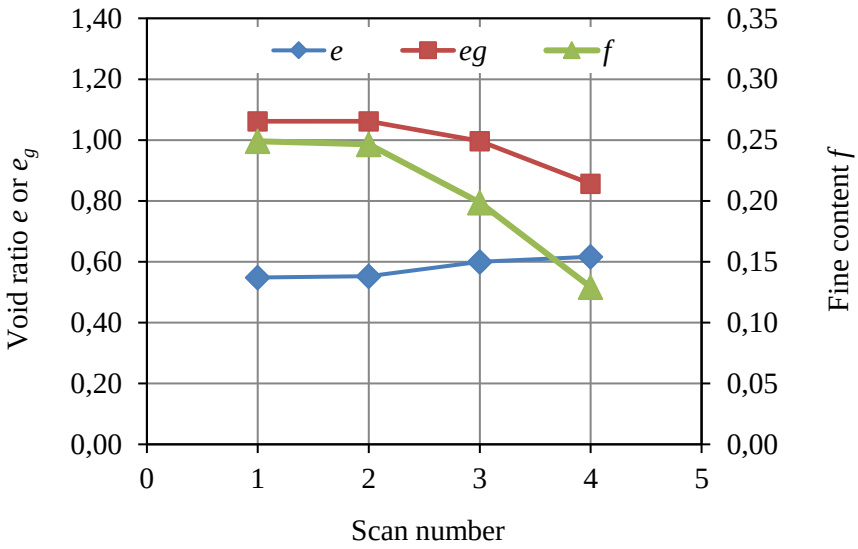

Fig. 10 Void ratio e, inter-granular void ratio e_g and fine content f of the 4 successive scans.

5.2 Local state and deformation

From the calibrated images presented previously, the sample can be meshed on a regular lattice to create meso-scale sub-volumes, each sub-volume including several voxels. Such sub-volumes will be used to define and compute local fines content, void ratio and inter-granular void ratio which cannot be defined at the scale of a single voxel (except for the fines content if the voxel belongs to the inter-granular space). The optimal size of the sub-volume is required so as to define a representative elementary volume (REV). For this purpose, the evolution of the inter-granular void ratio in scan 01 has been considered as a function of the mesh size (**Fig. 11**). The different curves stand for 20 distinct cube centers chosen randomly. The results show that beyond a mesh size of almost 50 px (4.5 mm), the inter-granular void ratio tends to some constant value, irrespectively of the chosen sub-volume size. The REV size for this material is consequently around 50 voxels or, equivalently, a little less than three times the median diameter D_{50} of the coarse grains.

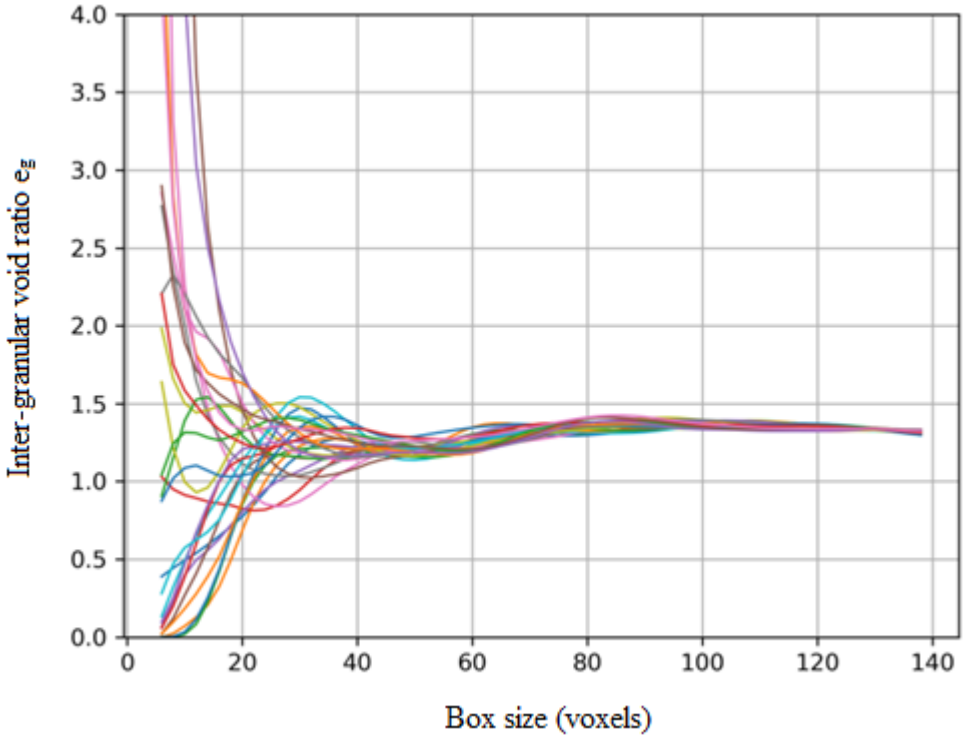

Fig. 11 Inter-granular void ratio versus the box size used for its calculation.

Fig. 12 shows the spatial fields of the different physical properties (e, e_g and f) of the soil sample during the erosion test in the median vertical plane; each point corresponds to a representative value averaged in a cube of side 50 px, representing 4.5 mm (i.e. the average is also performed in the direction orthogonal to the vertical plane shown in Fig. 12 over a length of 50 px). After preparing the sample, scan 01 reveal an almost homogeneous distribution of void ratio e, inter-granular void ratio e_g and fines content f without grain segregation. Besides, the initial homogeneous distribution of fines seems not to be affected by the saturation stage, performed before the 1st scan. Comparison of scans 01 and 02 confirms also that no noticeable erosion is observed at low flow rate. On the contrary, in scans 03 and 04, where suffusion occurred, there is a significant drop in fines content, especially at the circumferential edges of the sample, indicating that most of the fine particles removal remains mainly located at the periphery of the soil sample. This observation is probably due to edge effects. Despite the use of a rough transparent plastic sheet at the lateral wall (see Sec. 2.1), a rather flat boundary conditions subsists for the erosion cell and are responsible for a slightly looser stage of the soil at the vicinity of the lateral wall. This is indeed visible in the distribution of the void ratio e for scan 01 and 02 where both left and right vertical boundaries of the figure are slightly lighter (*i.e.*, looser according to the color scale) than the sample bulk. Consequently, preferential flow paths are initially present near the cell wall, and they are progressively strengthened as the flow rate increases.

As observed previously at the sample scale, the increase in void ratio is also directly correlated, at the REV scale to the decrease in fines content, although mitigated by an overall settlement of the specimen. Indeed, the void ratio is heterogeneous, but even if at the sample scale, the void ratio globally increases (and the sample becomes looser), it is not true everywhere locally. In the last scan, the sample is looser (*i.e.*, the

void ratio *e*) than initially on the periphery but it is slightly denser in some places in the bulk. On the contrary, the inter-granular void ratio seems only slightly affected by these surrounding preferential flows. Its initial rather homogeneous distribution within the sample remains almost unchanged, showing that erosion induces only an overall decrease of the inter-granular void ratio in the entire sample. A slight heterogeneity appears nonetheless in scan 04.

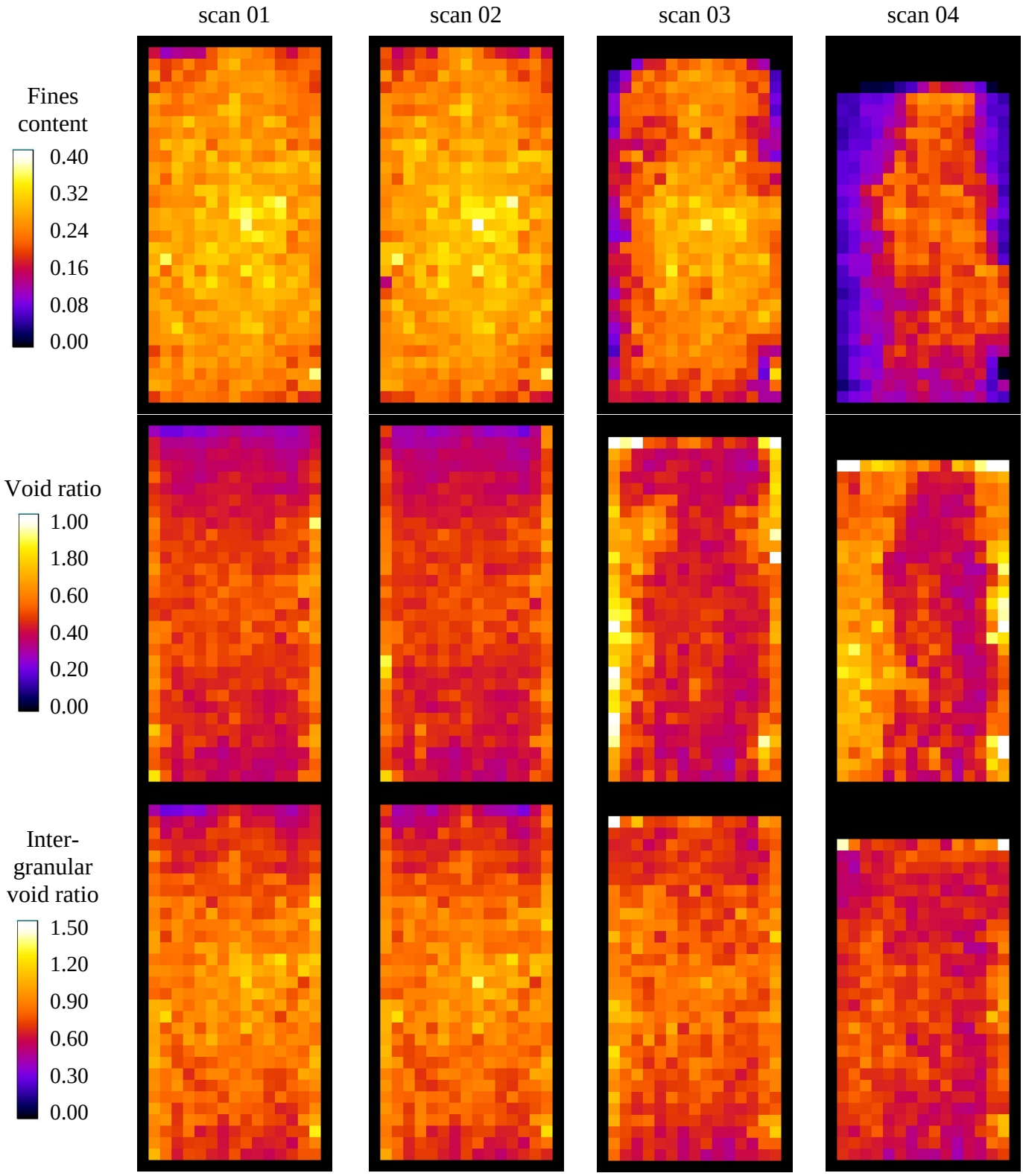

Fig. 12 Fields of fines content, void ratio and inter-granular void ratio in the median vertical plane of the 4 scans.

In the following paragraphs, the reconstructed images are used to perform volumetric Digital Image Correlation (DIC) in order to derive the displacement field and then the deformation fields related to the coarse granular phase. These specific image processing techniques are not described in this paper but details can be found in Tudisco *et al.* [36]. The code used here is the SPAM toolkit, currently under development. Inter-granular voids including fines are discarded in the image correlation processing as the displacement of fines may result from erosion process and is not representative, in this case, of the local deformation of the soil. In this objective, the binarised image obtained in the first step of the image processing (Fig. 7b) is used as a mask on the grey scale image (Fig. 7a) such that voxels (and their grey-level information) corresponding to the coarse grains are the only ones taken into account in the DIC. Incremental deformation fields (deformation fields between scans 1-2, scan 2-3, and scan 3-4) are calculated and the volumetric strain (first invariant of the strain tensor) and the intensity of the deviatoric strain (proportional to the second strain invariant) are presented in Fig. 13.

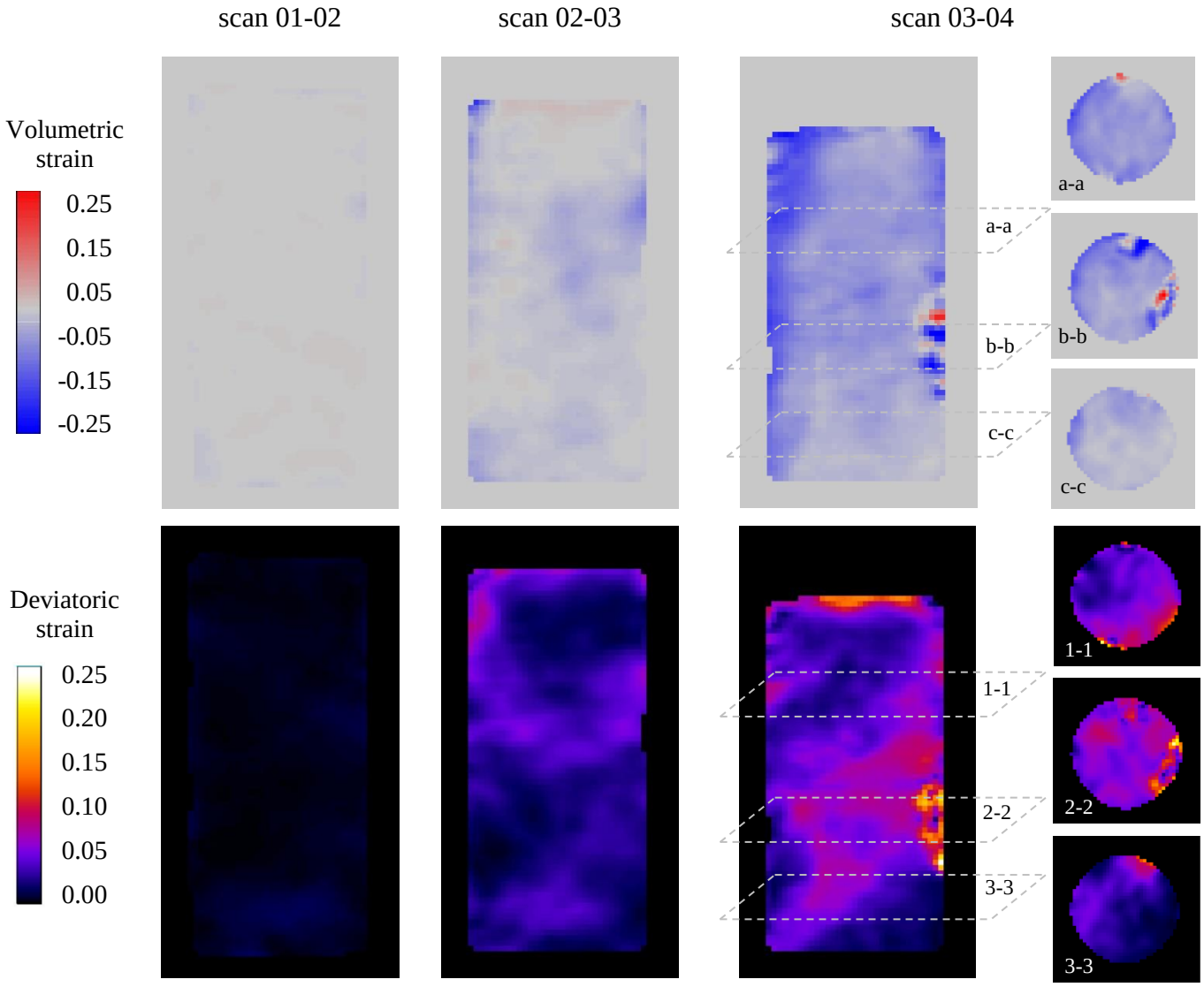

Fig. 13 Map of incremental volumetric and deviatoric strains in the median plane.

On volumetric strains maps, a negative volume deformation (in blue on the images) corresponds to a decrease in volume. As observed here, a significant volume decrease occurs at the periphery of the sample than in the center. This can be explained by a larger settlement in this zone owing to the rigidity of the cell and on the induced preferential paths at the periphery, as shown previously. This is also consistent with the bulging shape of the upper surface of the sample as shown in **Fig. 8**. On the increment 03-04, we observe very locally some volume increases (sections a-a and b-b). In some zones, close to the sample boundary, the convergence of the DIC algorithm was not total (because of relatively large displacements of the coarse grains at those places). Therefore, such local zones highly dilatant (associated to neighboring zone highly contractant) are an artefact of the DIC itself than representative of the actual volume change.

Concerning the incremental deviatoric strain field, it reveals more specifically the presence of shear strain. The shear strain remains at a rather low intensity within the specimen. The local high shear intensity near the sample boundaries, (in the same zones as the volume increases) should be discarded from the reasons given here above. Nevertheless, shearing develops in the bulk of the sample. This is consistent with the relatively higher peripheral settlement (compaction) which should accommodate with the lower settlement along the sample axis. In other words, due the heterogeneous development of suffusion, the soil sample does not experience a strict compaction in oedometric conditions but is also slightly sheared under its own weight.

5.3 Vertical profiles of fines content, void ratio and inter-granular void ratio

To obtain further quantitative results on the local physical properties (fines content f, void ratio e and inter-granular void ratio e_g), some space-averaging is implemented. First, all the f, e, and, e_g values in voxels located at a given height z are averaged in a horizontal slice of 30 voxels thickness to evaluate $f(z)$, $e(z)$, and $e_g(z)$, respectively. The corresponding vertical profiles of fine contents, void ratio and inter-granular void ratio, as well as the incremental variations of these parameters with respect to the previous scan are presented in **Fig. 14**.

Interestingly, the interfaces between the compacted layers by moist tamping method (depicted by dotted lines) are clearly visible on the profiles from scan 01 and scan 02, still distinguishable in scan 03 and ultimately disappear in scan 04 due to both the washout of the eroded fine particles and the substantial rearrangement of coarse grains. This implies that the sample preparation by moist tamping method does not really create a perfectly homogeneous sample with the obvious presence of layering, as previously demonstrated by Frost and Park [27]. An over-compaction is also observed in the upper layer and, to a lower degree, in the one immediately below. Regarding the fines content (**Fig. 14**a), there is a substantially smaller concentration in the top and the bottom layers. By analyzing the variation of the fines content between scan 01 and scan 02 (**Fig. 14**b), although it is confirmed that the global amount of fines content remains constant since the wash-out of the fines particles has not yet occurred in this step, some slight changes in the vertical distribution of the fines particles can be observed nonetheless. The most significant change is a migration of fines at the top of the sample towards the rest of the specimen. To understand this, it is worth recalling that scan 01 and scan 02 are respectively obtained after the saturation phase performed with an upward flow and after the phase of the flow reversal (downward) to carry out the erosion stages.

Indeed, during the saturation step, fine particles contained between (or surrounding) the coarse grains might fall downward for a certain distance at the wetting front during water infiltration into sample. Afterwards, it is likely that the change in the flow direction can rather easily re-mobilize these particles and consequently slightly modify the fines concentrations with an expected loss at the top of the sample and a general migration downward. From **Fig. 14**a, scans 03 and 04 are characterized by a significant drop in fines content throughout the entire sample height as erosion occurs, more pronounced in the two upper layers for scan 03 and roughly homogeneous for scan 04, except at the bottom of the sample where a lesser loss of fine particles is observed in both scans.

Regarding the evolution of the void ratio (**Fig. 14**c), it can be observed that, apart from the top of the sample, the void ratio varies only slightly throughout its height. This is to be attributed to a balance between the erosion of the fine particles and the settlement. Consistently, the inter-granular void ratio decreases more significantly due to the progressive collapse and reorganization of the coarse grains induced by the loss in fines and subsequent localized instabilities (**Fig. 14**e).

One should note that, with the exception of the discontinuities located at the transition between the different soil layers, there is not much heterogeneity induced by erosion along the vertical direction as shown by all these vertical profiles. Therefore, no local clogging of fine particles (that would be represented by a sharp increase of the fines concentration) was observed in any given horizontal sections.

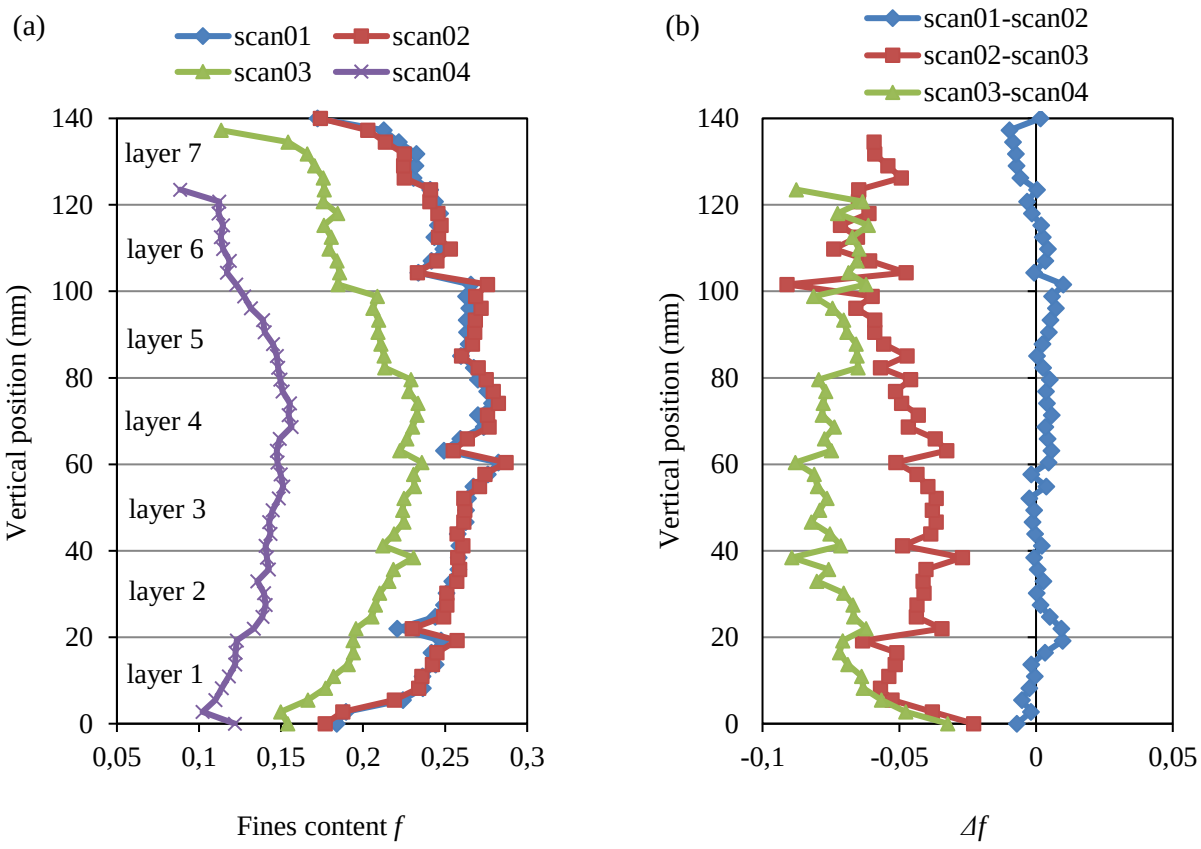

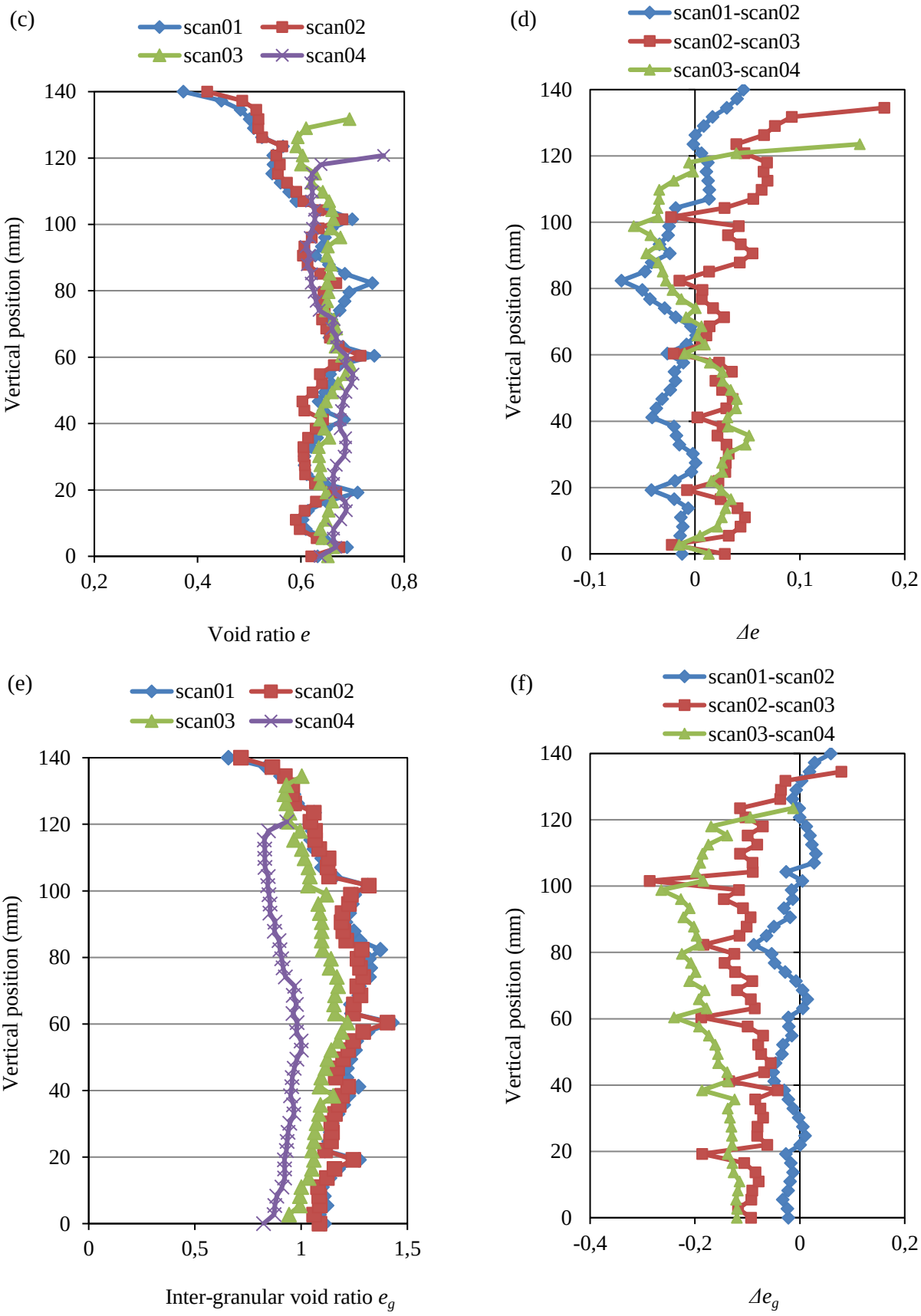

Fig. 14 Vertical profiles of: (a) fines content, (b) incremental variations of fines content, (c) void ratio, (d) incremental variations of void ratio, (e) inter-granular void ratio and (f) incremental variations of inter-granular void ratio of the 4 scans.

5.4 Radial profiles of fines content, void ratio and inter-granular void ratio

The physical properties of the soil (fines content f, void ratio e, inter-granular void ratio e_g) are now averaged at a radial distances r from the revolution axis of the sample in the volume between $r - \Delta r/2$ and $r + \Delta r/2$ (with Δr = 30 pixels). The corresponding radial profiles of $f(r)$, $e(r)$, and $e_g(r)$ and the incremental variations of these parameters with respect to the previous scan are plotted in **Fig. 15**.

The edge effects and related induced heterogeneities are clearly visible in all these radial profiles, even for scan 01. It can thus be noted that the preparation method, combining moist tamping (compaction control at the periphery) and saturation, fails to create a homogeneous sample in terms of radial distribution. A substantial lack of both fine particles and coarse grains occur at the lateral wall as revealed by a lower fine content and a higher inter-granular void ratio in scan 01. The evolution from scan 01 to scan 02 of fines content (**Fig. 15**a) is almost negligible, as expected though the flow rate was too low for erosion to occur. Only slight changes are observed at the lateral wall. In scans 03 and 04, where significant suffusion occurred, the loss in fine particles near the periphery is much higher compared to the one in the center and there is a rather progressive decrease of f as the radius increases. However, as regards the incremental change in fines content (**Fig. 15**b), scan 03 reveals a zone at the periphery where a high gradient in fines content increment is observed, whereas it remains almost constant in the central zone. Conversely, scan 04 displays a roughly constant and homogeneous distribution of the incremental change in fines. In other words, erosion of fine is strongly heterogeneous (with respect to the radial direction) in the increment 02-03 and then tends to become homogeneous in the increment 03-04.

Regarding the incremental evolution of the void ratio during erosion (**Fig. 15**d), it can be interestingly noted that, in the center of the sample, approximately for $r/R < 0.5$ (R: sample radius), the void ratio is slightly lower; the soil is generally in a slightly denser state. In this zone, the loss of fine appears to be slightly over-compensated by coarse grains settlements. The latter, as shown in the radial profiles of the inter-granular void ratio (**Fig. 15**e), occurs approximately in the same way everywhere in the sample since a roughly homogeneous decrease of Δe_g along the radial direction is observed.

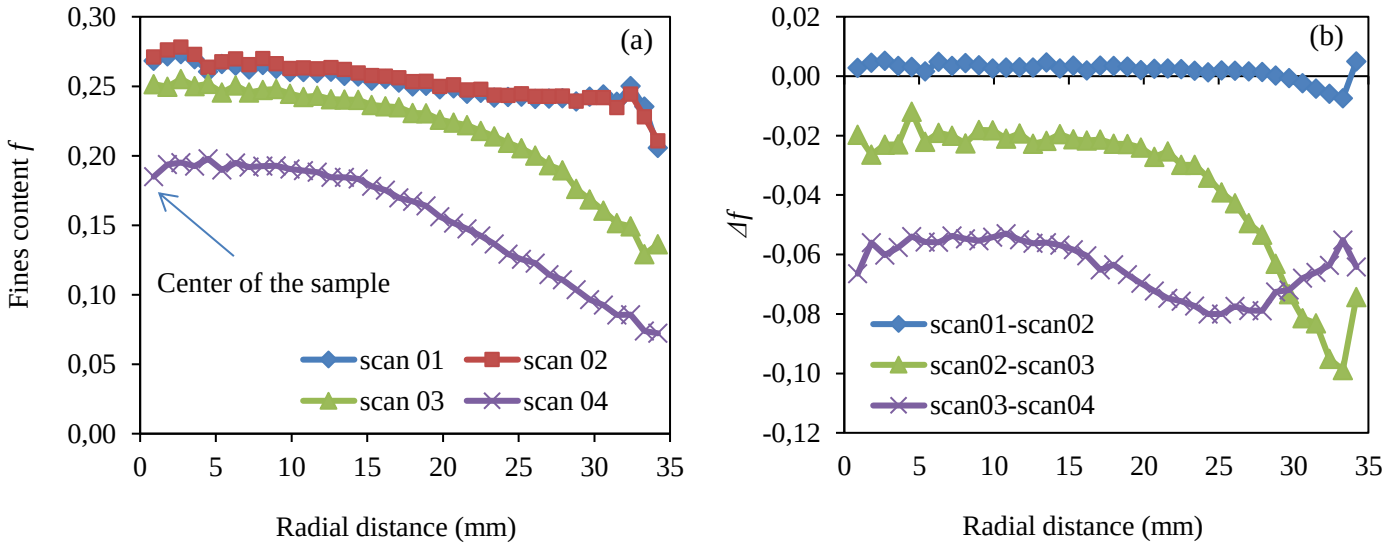

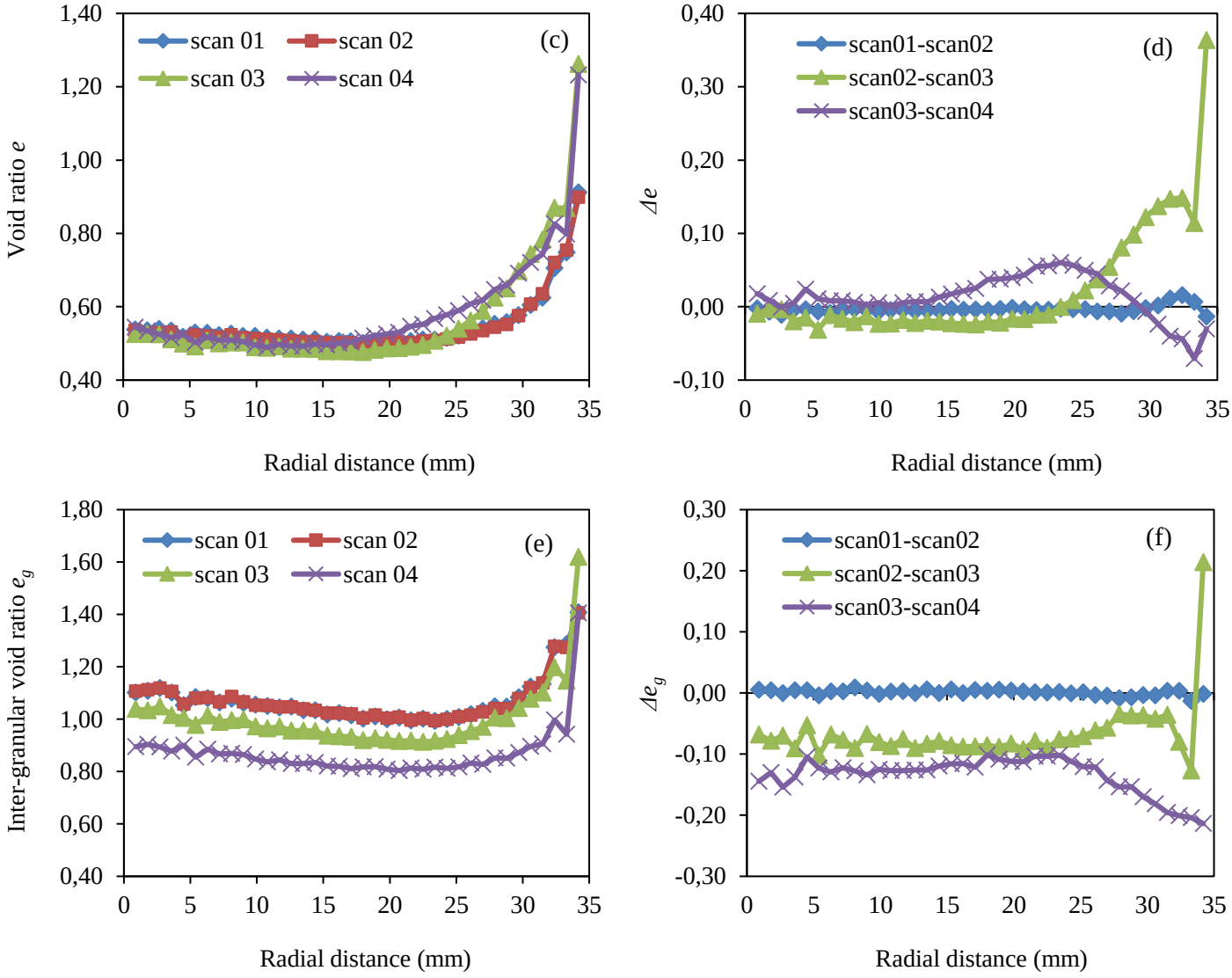

Fig. 15 Radial profiles of: (a) fines content, (b) incremental variations of fines content, (c) void ratio, (d) incremental variations of void ratio, (e) inter-granular void ratio and (f) incremental variations of inter-granular void ratio of the 4 scans.

6 Conclusion

In this study, x-ray tomography technique has been used to experimentally characterize the impact of suffusion on the soil micro-structure. The micro-structural changes during the suffusion process were accurately investigated in terms of strain fields and spatial distribution of fines content, void ratio and inter-granular void ratio through vertical and radial profiles. The following conclusions can be drawn.

From a practical perspective, it was demonstrated here that, for an x-ray CT of a gap-graded soil, a spatial resolution of images around half the median diameter of the fines particles (more precisely here a resolution of $0.43d_{50}$) was sufficient to measure the different physical properties (fines content, void ratio and inter-granular void ratio) with a high accuracy. This conclusion reinforces the potential of using x-ray CT data in complement to numerical results provided by discrete element methods (DEM) for instance and to mechanical tests at macro scale. These data could be very useful for interpreting, in a more objective and

coherent manner, the mechanical behavior of granular soils, especially the altered or destructured ones by erosion or other processes.

A secondary practical outcome of the present study is the confirmation that the moist tamping method fails, in a certain way, to create a reasonably homogeneous sample since it generates a microstructural stratification, in agreement with previous results on the subject.

The most important outcome here is clearly the occurrence of significant heterogeneities in the soil physical properties due to the suffusion process, as highlighted by the spatial maps of void ratio, inter-granular void ratio, and fines content. More precisely, the loss of fines is substantially higher at the periphery of the sample, suggesting some preferential flow paths. On the contrary, a roughly homogeneous suffusion process is observed along the flow direction, apart from the upper portion of the sample, at the interstitial flow inlet, and more marginally at the bottom of the sample. Interestingly, it also appears that, with greater erosion intensity, the loss of fines gets much more uniformly distributed within the sample, but without removing the radial heterogeneities previously induced at smaller flow rates. In the case studied in this paper, the heterogeneity of the sample was such that the part of the sample around its revolution axis was slightly denser after erosion than in the initial state whereas it was looser in the peripheral zones. This result comes by considering the whole solid phase (fines and coarse grains). Now, if only the coarse granular skeleton is considered, only a global compaction is observed. However, as this compaction is slightly more pronounced on periphery than in the center of the soil sample, the soil is somehow "pre-sheared" to accommodate this different volume changes in different zones. All this complex loading history experienced by the soil during the suffusion development make rather difficult the interpretation of post-erosion mechanical test (as triaxial compression) and even more the assessment, a priori, of the mechanical properties related to post-erosion physical state.

From a more general perspective, the existence of such pronounced heterogeneities, or even of localized singularities, is prone to question usual interpretations of suffusion tests at sample scale, where the soil structure is implicitly assumed to be homogeneous and where the erosion process is consequently expected to be uniform at the local scale. The same holds for the triaxial test, or other mechanical tests on eroded soil samples, whose results are used to determine the impact of suffusion on mechanical strength and predict a possible degradation of the shear resistance performance. Furthermore, the fact that these heterogeneities are likely to be induced by preferential flow paths nearby rigid walls of the testing cell also questions the relevance of characterizing the materials behavior with small-scale devices, having their own inherent edges, to be subsequently applied to large-scale situations with totally different boundary conditions.

Acknowledgements

A funding provided by Provence-Alpes-Côte d'Azur region is gratefully acknowledged as well as a fruitful partnership with the engineering company SAFEGE. The support of Grenoble Alpes University through the project ERODE (AGIR program) is also acknowledged. We thank P. Charrier and R. Aboul Hosn from Laboratoire 3SR, L.-H. Luu and A. Wautier from Irstea for the help provided during the realization of the

tests presented in this paper. We also would like to thank Professors D. Marot and Y. Khidas for their fruitful discussions.

References

1. Chang, D. and L. Zhang, *A stress-controlled erosion apparatus for studying internal erosion in soils.* Geotechnical Testing Journal, 2011. **34**(6): p. 579-589.
2. Xiao, M. and N. Shwiyhat, *Experimental investigation of the effects of suffusion on physical and geomechanic characteristics of sandy soils.* Geotech Testing J, 2012. **35**(6): p. 890-900.
3. Ke, L. and A. Takahashi, *Triaxial erosion test for evaluation of mechanical consequences of internal erosion.* Geotechnical Testing Journal, 2014. **37**(2).
4. Fell, R. and J.-J. Fry, *Internal Erosion of Dams and Their Foundations: Selected and Reviewed Papers from the Workshop on Internal Erosion and Piping of Dams and their Foundations, Aussois, France, 25–27 April 2005*. 2014: CRC Press.
5. Bonelli, S., *Erosion in geomechanics applied to dams and levees*. 2013: John Wiley & Sons.
6. Kenney, T. and D. Lau, *Internal stability of granular filters.* Canadian Geotechnical Journal, 1985. **22**(2): p. 215-225.
7. Li, M. and R.J. Fannin, *Comparison of two criteria for internal stability of granular soil.* Canadian Geotechnical Journal, 2008. **45**(9): p. 1303-1309.
8. Wan, C.F. and R. Fell, *Assessing the potential of internal instability and suffusion in embankment dams and their foundations.* Journal of geotechnical and geoenvironmental engineering, 2008.
9. Kézdi, Á., *Soil physics: selected topics*. Developments in geotechnical engineering. 1979.
10. Kenney, T. and D. Lau, *Internal stability of granular filters: Reply.* Canadian Geotechnical Journal, 1986. **23**(3): p. 420-423.
11. Burenkova, V., *Assessment of suffusion in non-cohesive and graded soils*, in *Filters in geotechnical and hydraulic engineering. Balkema, Rotterdam*1993. p. 357-360.
12. To, P., A. Scheuermann, and D. Williams, *Quick assessment on susceptibility to suffusion of continuously graded soils by curvature of particle size distribution.* Acta Geotechnica, 2018. **13**(5): p. 1241-1248.
13. Indraratna, B., A.K. Raut, and H. Khabbaz, *Constriction-based retention criterion for granular filter design.* Journal of Geotechnical and Geoenvironmental Engineering, 2007. **133**(3): p. 266-276.
14. Scheuermann, A. and J. Kiefer. *Internal erosion of granular materials–Identification of erodible fine particles as a basis for numerical calculations*. in *9th International Congress of the Hellenic Society of Theoretical and Applied Mechanics (HSTAM)*. 2010. Hellenic Society for Theoretical & Applied Mechanics (HSTAM).
15. Moraci, N., M.C. Mandaglio, and D. Ielo, *A new theoretical method to evaluate the internal stability of granular soils.* Canadian Geotechnical Journal, 2011. **49**(1): p. 45-58.
16. Marot, D., F. Bendahmane, and H.H. Nguyen, *Influence of angularity of coarse fraction grains on internal erosion process.* La Houille Blanche, 2012(6): p. 47-53.
17. Bendahmane, F., D. Marot, and A. Alexis, *Experimental parametric study of suffusion and backward erosion.* Journal of Geotechnical and Geoenvironmental Engineering, 2008. **134**(1): p. 57-67.
18. Moffat, R. and R.J. Fannin, *A hydromechanical relation governing internal stability of cohesionless soil.* Canadian Geotechnical Journal, 2011. **48**(3): p. 413-424.
19. Skempton, A. and J. Brogan, *Experiments on piping in sandy gravels.* Geotechnique, 1994. **44**(3): p. 449-460.
20. Moffat, R., R.J. Fannin, and S.J. Garner, *Spatial and temporal progression of internal erosion in cohesionless soil.* Canadian Geotechnical Journal, 2011. **48**(3): p. 399-412.
21. Hosn, R.A., et al. *Microscale analysis of the effect of suffusion on soil mechanical properties*. in *International Workshop on Bifurcation and Degradation in Geomaterials*. 2017. Springer.
22. Sail, Y., et al., *Suffusion tests on cohesionless granular matter: Experimental study.* European Journal of Environmental and Civil Engineering, 2011. **15**(5): p. 799-817.
23. Luo, Y.-l., et al., *Hydro-mechanical experiments on suffusion under long-term large hydraulic heads.* Natural hazards, 2013. **65**(3): p. 1361-1377.

24. Israr, J., B. Indraratna, and C. Rujikiatkamjorn, *Laboratory investigation of the seepage induced response of granular soils under static and cyclic loading.* Geotechnical Testing Journal, 2016. **39**(5): p. 795-812.
25. Bianchi, F., et al., *Tomographic Study of Internal Erosion of Particle Flows in Porous Media.* Transport in Porous Media, 2018. **122**(1): p. 169-184.
26. Mehdizadeh, A. and M. Disfani, *Micro Scale Study of Internal Erosion using 3D X-Ray Tomography*. 2018.
27. Frost, J. and J. Park, *A critical assessment of the moist tamping technique.* Geotechnical Testing Journal, 2003. **26**(1): p. 57-70.
28. Benahmed, N., J. Canou, and J.-C. Dupla, *Structure initiale et propriétés de liquéfaction statique d un sable*. Comptes rendus mécanique, 2004. **332**(11): p. 887-894.
29. Desrues, J., et al., *Void ratio evolution inside shear bands in triaxial sand specimens studied by computed tomography*. Géotechnique, 1996. **46**(3): p. 529-546.
30. Hasan, A. and K. Alshibli, *Experimental assessment of 3D particle-to-particle interaction within sheared sand using synchrotron microtomography.* Géotechnique, 2010. **60**(5): p. 369.
31. Hall, S., et al., *Discrete and continuum analysis of localised deformation in sand using X-ray [mu] CT and volumetric digital image correlation.* Géotechnique, 2010. **60**(5): p. 315.
32. Homberg, U., et al., *Automatic extraction and analysis of realistic pore structures from µct data for pore space characterization of graded soil.* 2012.
33. Fonseca, J., et al., *Microstructural analysis of sands with varying degrees of internal stability.* Géotechnique, 2014. **64**(5): p. 405-411.
34. Dumberry, K., F. Duhaime, and Y.A. Ethier, *Erosion monitoring during core overtopping using a laboratory model with digital image correlation and X-ray microcomputed tomography.* Canadian Geotechnical Journal, 2017. **55**(2): p. 234-245.
35. Hosn, R.A., et al. *Effects of Suffusion on the Soil's Mechanical Behavior: Experimental Investigations*. in *European Working Group on Internal Erosion*. 2018. Springer.
36. Tudisco, E., et al., *TomoWarp2: a local digital volume correlation code.* SoftwareX, 2017. **6**: p. 267-270.